DIFFERENT KINDS OF MODULUS–MODULUS SYNCHRONIZATION FOR CHAOTIC COMPLEX SYSTEMS AND THEIR APPLICATIONS

Gamal M. Mahmoud[a], Hesham Khalaf[a], Mohamed M. Darwish[b]
Tarek M. Abed-Elhameed[a]

[a]Department of Mathematics, Faculty of Science, Assiut University
Assiut 71516, Egypt
[b]Department of Computer Science, Faculty of Computers and Information
Assiut University, Assiut 71516, Egypt

Received 9 January 2022, accepted 5 May 2022,
published online 6 June 2022

The definitions of the complete modulus–modulus synchronization (CMMS), modulus–modulus combination synchronization (MMCS), and modulus–modulus combination–combination synchronization (MMCCS) for chaotic complex systems are introduced. These types of synchronization may be considered as a generalization of many other types of synchronization in the literature. Based on the active control method, three schemes are stated to achieve: CMMS, MMCS, and MMCCS. Three theorems are presented and proved to provide us with analytical formulas for the control functions. We present examples to test the validity of the control functions to achieve CMMS, MMCS, and MMCCS. Using the Runge–Kutta of the order of 4 method, we got the numerical solutions of our systems which agree well with the analytical results. Based on the CMMS of two chaotic complex systems, the processes of encryption and decryption of images are introduced. The experimental results of image encryption and decryption as well as the information entropy and histograms are calculated. Similar studies using MMCS and MMCCS are also investigated.

DOI:10.5506/APhysPolB.53.6-A2

1. Introduction

Chaos synchronization has been studied for the first time in 1990 [1]. The trajectory of a chaotic real system is not simple due to the sensitivity of its initial condition. Many researchers gave much attention to this phenomenon. Pecora and Carroll presented the complete synchronization [1], while the anti synchronization was given by Kim *et al.* [2]. Mainieri *et al.* [3] studied the projective synchronization and the modified projective synchronization was considered by Li [4]. Li *et al.* [5] investigated the lag synchronization, while the function synchronization is illustrated in [6]. The combination synchronization is introduced in [7, 8] and the combination–combination synchronization is presented in [8, 9]. Sun *et al.* investigated the compound combination synchronization [10], while the double compound combination synchronization was given by Mahmoud *et al.* [11]. Recently, Li *et al.* [12] introduced the complete modulus synchronization between hyperchaotic real and complex systems. Using the adaptive control, Khan and Nigar [13] studied the modulus combination–combination synchronization and they used this technique in secure communication. Chaos synchronization is used in the cryptosystems, which are mainly applied in encrypting text message, the sine and cosine signal, sound signal, gray and color images, and so on [14–17]. Encryption schemes based on chaotic and hyperchaotic systems have the advantage of introducing a good combination of security and speed [18]. Many schemes of image encryption have been presented with different properties and motivations for application based on chaotic systems (*e.g.* see [17–21] and references therein).

In [22], Mahmoud *et al.* investigated the complex Chen system, which is

$$\begin{aligned} \dot{x_1} &= a_1(x_2 - x_1)\,, \\ \dot{x_2} &= (a_2 - a_1)x_1 - x_1x_3 + a_2x_2\,, \\ \dot{x_3} &= \tfrac{1}{2}(\bar{x}_1x_2 + \bar{x}_2x_1) - a_3x_3\,, \end{aligned} \tag{1}$$

where a_1, a_2, and a_3 are positive real parameters, $x_1 = x_1^r + jx_1^i$, $x_2 = x_2^r + jx_2^i$ are complex variables, $j = \sqrt{-1}$ and x_3 is real one. The time derivatives are denoted by dots, while the complex conjugate variable is represented by $(.\bar{.}.)$.

In 1982, the Lorenz system in the complex domain was discovered from laser physics and baroclinic instability of the geophysical flows [23–26] as

$$\begin{aligned} \dot{y_1} &= \sigma(y_2 - y_1)\,, \\ \dot{y_2} &= ry_1 - y_1y_3 - ay_2\,, \\ \dot{y_3} &= \tfrac{1}{2}(\bar{y}_1y_2 + y_1\bar{y}_2) - by_3\,, \end{aligned} \tag{2}$$

where r and a are complex numbers defined as $r = r_1 - jr_2$ and $a = 1 - j\delta$, $j = \sqrt{-1}$ and σ, r_1, r_2, δ, and b are real positive parameters. The complex variables y_1, y_2, and the real variable y_3 of system (2) have relations with the electric field, the atomic polarization amplitudes, and the population inversion in a ring laser system of two-level atoms respectively [27].

The authors of Ref. [22] introduced the complex Lü system as

$$\begin{aligned} \dot{z_1} &= c_1(z_2 - z_1)\,, \\ \dot{z_2} &= -z_1z_3 + c_2z_2\,, \\ \dot{z_3} &= \tfrac{1}{2}(\bar{z}_1z_2 + \bar{z}_2z_1) - c_3z_3\,, \end{aligned} \tag{3}$$

where c_1, c_2, and c_3 are positive real parameters, z_1, z_2 are complex variables, and z_3 is real.

The equations for the complex Rössler system [28] are as follows:

$$\begin{aligned}\dot{w}_1 &= -w_1 - w_3\,,\\ \dot{w}_2 &= w_1 + d_1 w_2\,,\\ \dot{w}_3 &= d_2 + \tfrac{1}{2} w_3 (w_1 + \bar{w}_1 - 2d_3)\,,\end{aligned} \tag{4}$$

where the variables w_1, w_2 are complex, and w_3 is real. The parameters d_1, d_2, and d_3 are real positive parameters.

In this article, we introduce the definitions of the CMMS, MMCS, and MMCCS for chaotic complex systems. Three schemes are stated to achieve CMMS, MMCS, and MMCCS using the active control technique [22]. We presented and proved three theorems to provide us with analytical expressions for the control functions. The chaotic complex Chen, Lorenz, Lü, and Rössler systems (1)–(4) are used as examples to test the validity of the control functions to achieve CMMS, MMCS, and MMCCS. There exists a good agreement between analytical results and numerical simulations. Based on the CMMS between chaotic complex Chen and Lorenz systems, the processes of encryption and decryption of images are introduced. The histograms and the information entropy are calculated for images.

The arrangement of our article is as follows: In Section 2, the definitions of the CMMS, MMCS, and MMCCS of chaotic complex systems are introduced. We state and prove three theorems to provide us with analytical formulas for the control functions. Examples to demonstrate the good agreement between analytical and numerical results are presented in Section 3. The steps of the process of encryption and decryption of images based on CMMS between complex Chen and Lorenz systems are stated in Section 4. The grayscale histograms and information entropy are computed for the images of this work. Other applications of images encryption and decryption using the MMCS and MMCCS of chaotic complex systems can be similarly studied. Section 5 contains the conclusions of our investigations.

2. Three kinds of modulus–modulus synchronization between chaotic complex systems

In this section, we introduce three new definitions of modulus–modulus synchronization which are CMMS, MMCS, and MMCCS for chaotic (or hyperchaotic) complex dynamical systems. We state and prove theorems to yield the analytical formulas for the control functions to achieve these kinds of synchronization using an active control method.

2.1. Complete modulus–modulus synchronization (CMMS) between two chaotic complex systems

This subsection deals with the CMMS of chaotic complex systems. The drive and response systems, respectively, are

$$\dot{x} = f(x)\,, \qquad x \in \boldsymbol{C^n}\,, \tag{5}$$

where $f(x) = f^r(x) + jf^i(x)$, $x = x^r + jx^i$, with $x^r = (x_1^r, x_2^r, \ldots, x_n^r)^{\mathrm{T}}$, $x^i = (x_1^i, x_2^i, \ldots, x_n^i)^{\mathrm{T}}$,

$$\dot{y} = g(y) + u\,, \qquad y, u \in \boldsymbol{C^n}\,, \tag{6}$$

where $g(y) = g^r(y) + jg^i(y)$, $y = y^r + jy^i$, with $y^r = (y_1^r, y_2^r, \ldots, y_n^r)^{\mathrm{T}}$, $y^i = (y_1^i, y_2^i, \ldots, y_n^i)^{\mathrm{T}}$, $u = u^r + ju^i$, with $u^r = (u_1^r, u_2^r, \ldots, u_n^r)^{\mathrm{T}}$, $u^i = (u_1^i, u_2^i, \ldots, u_n^i)^{\mathrm{T}}$ is the vector of control functions which are functions of x, y, and T denotes the transpose.

Definition 2.1. CMMS between the drive system (5) and the response system (6) is achieved if

$$\lim_{t\to\infty} \|e\| = \lim_{t\to\infty} \||y| - |x|\| = 0\,, \qquad e = (e_1, e_2, \ldots, e_n)^{\mathrm{T}} \tag{7}$$

and

$$e_l = |y_l| - |x_l| = \sqrt{\left(y_l^r\right)^2 + \left(y_l^i\right)^2} - \sqrt{\left(x_l^r\right)^2 + \left(x_l^i\right)^2}\,, \qquad l = 1, 2, \ldots, n\,, \tag{8}$$

where $\|\cdot\|$ is the norm and $e \in \boldsymbol{R}^n$ is the synchronization error.

Remark 2.2. For real variable y in (7), we get the modulus synchronization [12], so Definition 2.1 can be considered as a generalization of modulus synchronization of Ref. [12].

Theorem 2.3. *CMMS will be carried out for the drive system (5) and the response system (6) if the control functions are designed as follows:*

$$u_l^r = -g^r(y_l) + \frac{\sqrt{\left(y_l^r\right)^2 + \left(y_l^i\right)^2}}{y_l^r}\left(\frac{x_l^r f^r(x_l)}{\sqrt{\left(x_l^r\right)^2 + \left(x_l^i\right)^2}} - A_l e_l\right), \quad l = 1, 2, \ldots, n\,, \tag{9}$$

$$u_l^i = -g^i(y_l) + \frac{\sqrt{\left(y_l^r\right)^2 + \left(y_l^i\right)^2}}{\sqrt{\left(x_l^r\right)^2 + \left(x_l^i\right)^2}}\,\frac{x_l^i f^i(x_l)}{y_l^i}\,, \quad l = 1, 2, \ldots, n\,, \tag{10}$$

where $\mathrm{diag}(A_1, A_2, \ldots, A_n) = K_1$ *is the feedback gain matrix with positive eigenvalues.*

Proof. By differentiating the synchronization errors (8) w.r.t. t, we get

$$\dot{e}_l = \frac{y_l^r \dot{y}_l^r + y_l^i \dot{y}_l^i}{\sqrt{\left(y_l^r\right)^2 + \left(y_l^i\right)^2}} - \frac{x_l^r \dot{x}_l^r + x_l^i \dot{x}_l^i}{\sqrt{\left(x_l^r\right)^2 + \left(x_l^i\right)^2}} \,. \tag{11}$$

Substituting Eqs. (5)–(6) into Eq. (11), we have

$$\begin{aligned} \dot{e}_l \;=\; & \frac{y_l^r}{\sqrt{\left(y_l^r\right)^2 + \left(y_l^i\right)^2}} \left(g^r(y_l) + u_l^r\right) + \frac{y_l^i}{\sqrt{\left(y_l^r\right)^2 + \left(y_l^i\right)^2}} \left(g^i(y_l) + u_l^i\right) \\ & - \frac{x_l^r f^r(x_l)}{\sqrt{\left(x_l^r\right)^2 + \left(x_l^i\right)^2}} - \frac{x_l^i f^i(x_l)}{\sqrt{\left(x_l^r\right)^2 + \left(x_l^i\right)^2}} \,. \end{aligned} \tag{12}$$

Using Eqs. (9)–(10) and Eq. (12), we get

$$\dot{e} = -K_1 e \,. \tag{13}$$

The Lyapunov function is defined as

$$V(t) = \frac{1}{2} e^2 \,, \tag{14}$$

the time derivative of $V(t)$ is calculated as follows:

$$\dot{V}(t) = e\dot{e} = -K_1 e^2 \leq -\xi_{\min} \|e\|^2 < 0 \,, \tag{15}$$

where $\xi_{\min} = \min(\xi_1, \xi_2, \ldots, \xi_n) > 0$ is the minimum value of the eigenvalues of K_1. Then, $\lim\limits_{t\to\infty} \|e\| = 0$, and hence the CMMS between the drive system (5) and the response system (6) can be done. □

2.2. Modulus–modulus combination synchronization (MMCS) between three chaotic complex systems

The MMCS of chaotic complex systems with two drive and one response complex systems is investigated in this subsection. We consider the two drive complex systems as

$$\begin{aligned} \dot{x} &= f(x), \qquad x \in \boldsymbol{C}^{\boldsymbol{n}} \,, \\ \dot{y} &= g(y), \qquad y \in \boldsymbol{C}^{\boldsymbol{n}} \,, \end{aligned} \tag{16}$$

where $f(x) = f^r(x) + jf^i(x)$, $x = x^r + jx^i$, with $x^r = (x_1^r, x_2^r, \ldots, x_n^r)^{\mathrm{T}}$, $x^i = (x_1^i, x_2^i, \ldots, x_n^i)^{\mathrm{T}}$, $g(y) = g^r(y) + jg^i(y)$, $y = y^r + jy^i$, with $y^r = (y_1^r, y_2^r, \ldots, y_n^r)^{\mathrm{T}}$, $y^i = (y_1^i, y_2^i, \ldots, y_n^i)^{\mathrm{T}}$ and $j = \sqrt{-1}$.

The response complex system takes the form of

$$\dot{z} = h(z) + u\,, \qquad z, u \in \boldsymbol{C^n}\,, \tag{17}$$

where $h(z) = h^r(z) + jh^i(z)$, $z = z^r + jz^i$, with $z^r = (z_1^r, z_2^r, \ldots, z_n^r)^{\mathrm{T}}$, $z^i = (z_1^i, z_2^i, \ldots, z_n^i)^{\mathrm{T}}$, $u = u^r + ju^i$, with $u^r = (u_1^r, u_2^r, \ldots, u_n^r)^{\mathrm{T}}$, $u^i = (u_1^i, u_2^i, \ldots, u_n^i)^{\mathrm{T}}$ is the vector of control functions which are functions of x, y, z.

Definition 2.4. Two drive systems (16) and the response system (17) can achieve MMCS if

$$\lim_{t\to\infty} \|e\| = \lim_{t\to\infty} \||z| - |x+y|\| = 0\,, \qquad e = (e_1, e_2, \ldots, e_n)^{\mathrm{T}} \tag{18}$$

and

$$\begin{aligned} e_l &= |z_l| - |x_l + y_l| = \sqrt{\left(z_l^r\right)^2 + \left(z_l^i\right)^2} - \sqrt{\left(x_l^r + y_l^r\right)^2 + \left(x_l^i + y_l^i\right)^2}\,, \\ l &= 1, 2, \ldots, n\,, \end{aligned} \tag{19}$$

where $\|\cdot\|$ is the norm and $e \in \boldsymbol{R}^n$ is the synchronization error.

Remark 2.5. If z is a real variable in (18), we obtain the modulus combination synchronization [13].

Theorem 2.6. *The MMCS for the two drive systems (16) and the response system (17) can be carried out if the control functions are built as follows:*

$$\begin{aligned} u_l^r &= -h^r(z_l) + \frac{\sqrt{\left(z_l^r\right)^2 + \left(z_l^i\right)^2}}{z_l^r} \left(\frac{\left(x_l^r + y_l^r\right)\left(f^r(x_l) + g^r(y_l)\right)}{\sqrt{\left(x_l^r + y_l^r\right)^2 + \left(x_l^i + y_l^i\right)^2}} - B_l e_l \right), \\ l &= 1, 2, \ldots, n\,, \end{aligned} \tag{20}$$

$$\begin{aligned} u_l^i &= -h^i(z_l) + \frac{\sqrt{\left(z_l^r\right)^2 + \left(z_l^i\right)^2}}{z_l^i} \left(\frac{\left(x_1^i + y_1^i\right)\left(f^i(x_l) + g^i(y_l)\right)}{\sqrt{\left(x_l^r + y_l^r\right)^2 + \left(x_l^i + y_l^i\right)^2}} \right), \\ l &= 1, 2, \ldots, n\,, \end{aligned} \tag{21}$$

where $\mathrm{diag}(B_1, B_2, \ldots, B_n) = K_2$ *is the feedback gain matrix with positive eigenvalues.*

Proof. Differentiating (19) w.r.t. t, we obtain

$$\dot{e}_l = \frac{z_l^r \dot{z}_l^r + z_l^i \dot{z}_l^i}{\sqrt{\left(z_l^r\right)^2 + \left(z_l^i\right)^2}} - \frac{\left(x_l^r + y_l^r\right)\left(\dot{x}_l^r + \dot{y}_l^r\right) + \left(x_l^i + y_l^i\right)\left(\dot{x}_l^i + \dot{y}_l^i\right)}{\sqrt{\left(x_l^r + y_l^r\right)^2 + \left(x_l^i + y_l^i\right)^2}}\,. \tag{22}$$

Substituting Eqs. (16)–(17) into Eq. (22), we have

$$\begin{aligned}\dot{e}_l &= \frac{z_l^r}{\sqrt{\left(z_l^r\right)^2+\left(z_l^i\right)^2}}\left(h^r(z_l)+u_l^r\right)+\frac{z_l^i}{\sqrt{\left(z_l^r\right)^2+\left(z_l^i\right)^2}}\left(h^i(z_l)+u_l^i\right)\\ &\quad-\frac{\left(x_l^r+y_l^r\right)\left(f^r(x_l)+g^r(y_l)\right)+\left(x_l^i+y_l^i\right)\left(f^i(x_l)+g^i(y_l)\right)}{\sqrt{\left(x_l^r+y_l^r\right)^2+\left(x_l^i+y_l^i\right)^2}}\,.\end{aligned} \tag{23}$$

Using Eqs. (20)–(21) and Eq. (23), we get

$$\dot{e}=-K_2e\,. \tag{24}$$

One defines a Lyapunov function as

$$V(t)=\frac{1}{2}e^2\,, \tag{25}$$

the time derivative of $V(t)$ is given by

$$\dot{V}(t)=e\dot{e}=-K_2e^2\leq-\xi_{\min}\|e\|^2<0\,, \tag{26}$$

where $\xi_{\min}=\min(\xi_1,\xi_2,\ldots,\xi_n)>0$ is the minimum value of the eigenvalues of K_2. Then, $\lim\limits_{t\to\infty}\|e\|=0$, and hence the MMCS between the two drive systems (16) and the response system (17) can be achieved. □

2.3. Modulus–modulus combination–combination synchronization (MMCCS) between four chaotic complex systems

The MMCCS of chaotic complex systems between two drive and two response complex systems is stated. The two drive complex systems can be written as

$$\begin{aligned}\dot{x} &= f(x)\,, \qquad x,\in \boldsymbol{C^n}\,,\\ \dot{y} &= g(y)\,, \qquad y,\in \boldsymbol{C^n}\,,\end{aligned} \tag{27}$$

where $f(x)=f^r(x)+jf^i(x)$, $x=x^r+jx^i$, with $x^r=(x_1^r,x_2^r,\ldots,x_n^r)^{\mathrm{T}}$, $x^i=(x_1^i,x_2^i,\ldots,x_n^i)^{\mathrm{T}}$, $g(y)=g^r(y)+jg^i(y)$, $y=y^r+jy^i$, with $y^r=(y_1^r,y_2^r,\ldots,y_n^r)^{\mathrm{T}}$, $y^i=(y_1^i,y_2^i,\ldots,y_n^i)^{\mathrm{T}}$ and $j=\sqrt{-1}$.

The two response complex systems can be given as

$$\begin{aligned}\dot{z} &= h(z)+u\,, \qquad z,u\in \boldsymbol{C^n}\,,\\ \dot{w} &= s(w)+v\,, \qquad w,v\in \boldsymbol{C^n}\,,\end{aligned} \tag{28}$$

where $h(z) = h^r(z) + jh^i(z)$, $z = z^r + jz^i$, with $z^r = (z_1^r, z_2^r, \ldots, z_n^r)^{\mathrm{T}}$, $z^i = (z_1^i, z_2^i, \ldots, z_n^i)^{\mathrm{T}}$, $s(w) = s^r(w) + js^i(w)$, $w = w^r + jw^i$, with $w^r = (w_1^r, w_2^r, \ldots, w_n^r)^{\mathrm{T}}$, $w^i = (w_1^i, w_2^i, \ldots, w_n^i)^{\mathrm{T}}$, $u = u^r + ju^i$, with $u^r = (u_1^r, u_2^r, \ldots, u_n^r)^{\mathrm{T}}$, $u^i = (u_1^i, u_2^i, \ldots, u_n^i)^{\mathrm{T}}$, and $v = v^r + jv^i$, with $v^r = (v_1^r, v_2^r, \ldots, v_n^r)^{\mathrm{T}}$, $v^i = (v_1^i, v_2^i, \ldots, v_n^i)^{\mathrm{T}}$ are the vectors of control functions which are functions of x, y, z, w.

Definition 2.7. The MMCCS between two drive systems (27) and two response systems (28) can be achieved if

$$\lim_{t\to\infty} \|e\| = \lim_{t\to\infty} \||z+w| - |x+y|\| = 0\,, \qquad e = (e_1, e_2, \ldots, e_n)^{\mathrm{T}} \tag{29}$$

and

$$\begin{aligned} e_l &= |z_l + w_l| - |x_l + y_l| \\ &= \sqrt{\left(z_l^r + w_l^r\right)^2 + \left(z_l^i + w_l^i\right)^2} - \sqrt{\left(x_l^r + y_l^r\right)^2 + \left(x_l^i + y_l^i\right)^2}\,, \\ l &= 1, 2, \ldots, n\,, \end{aligned} \tag{30}$$

where $\|\cdot\|$ is the norm and $e \in \boldsymbol{R}^n$ is the synchronization error.

Remark 2.8. If z and w are real variables in (29), we get the modulus combination–combination synchronization [13].

Theorem 2.9. *MMCCS will be done for the two drive systems (27) and the two response systems (28) if the control functions are chosen as follows:*

$$\begin{aligned} u_l^r + v_l^r &= -\left(h^r(z_l) + s^r(w_l)\right) + \frac{\sqrt{\left(z_l^r + w_l^r\right)^2 + \left(z_l^i + w_l^i\right)^2}}{z_l^r + w_l^r} \\ &\quad \times \left(\frac{\left(x_l^r + y_l^r\right)\left(f^r(x_l) + g^r(y_l)\right)}{\sqrt{\left(x_l^r + y_l^r\right)^2 + \left(x_l^i + y_l^i\right)^2}} - C_l e_l \right), \qquad l = 1, 2, \ldots, n\,, \end{aligned} \tag{31}$$

$$\begin{aligned} u_l^i + v_l^i &= -\left(h^i(z_l) + s^i(w_l)\right) + \frac{\sqrt{\left(z_l^r + w_l^r\right)^2 + \left(z_l^i + w_l^i\right)^2}}{z_l^i + w_l^i} \\ &\quad \times \left(\frac{\left(x_l^i + y_l^i\right)\left(f^i(x_l) + g^i(y_l)\right)}{\sqrt{\left(x_l^r + y_l^r\right)^2 + \left(x_l^i + y_l^i\right)^2}} \right), \qquad l = 1, 2, \ldots, n\,, \end{aligned} \tag{32}$$

where $\mathrm{diag}(C_1, C_2, \ldots, C_n) = K_3$ *is the feedback gain matrix with positive eigenvalues.*

Proof. Differentiating (30) w.r.t. t, we obtain

$$\dot{e}_l = \frac{(z_l^r + w_l^r)(\dot{z}_l^r + \dot{w}_l^r) + (z_l^i + w_l^i)(\dot{z}_l^i + \dot{w}_l^i)}{\sqrt{(z_l^r + w_l^r)^2 + (z_l^i + w_l^i)^2}} - \frac{(x_l^r + y_l^r)(\dot{x}_l^r + \dot{y}_l^r) + (x_l^i + y_l^i)(\dot{x}_l^i + \dot{y}_l^i)}{\sqrt{(x_l^r + y_l^r)^2 + (x_l^i + y_l^i)^2}} . \tag{33}$$

Substituting Eqs. (27)–(28) into Eq. (33), we have

$$\dot{e}_l = \frac{(z_l^r+w_l^r)(h^r(z_l)+s^r(w_l)+u_l^r+v_l^r)+(z_l^i+w_l^i)(h^i(z_l)+s^i(w_l)+u_l^i+v_l^i)}{\sqrt{(z_l^r+w_l^r)^2+(z_l^i+w_l^i)^2}} - \frac{(x_l^r + y_l^r)(f^r(x_l) + g^r(y_l)) + (x_l^i + y_l^i)(f^i(x_l) + g^i(y_l))}{\sqrt{(x_l^r + y_l^r)^2 + (x_l^i + y_l^i)^2}} . \tag{34}$$

Using Eqs. (31)–(32) and Eq. (34), we get

$$\dot{e} = -K_3 e . \tag{35}$$

The Lyapunov function is defined as follows:

$$V(t) = \frac{1}{2}e^2 , \tag{36}$$

the time derivative of $V(t)$ is given by

$$\dot{V}(t) = e\dot{e} = -K_3 e^2 \le -\xi_{\min}\|e\|^2 < 0 , \tag{37}$$

where $\xi_{\min} = \min(\xi_1, \xi_2, \ldots, \xi_n) > 0$ is the minimum value of the eigenvalues of K_3. Then, $\lim_{t\to\infty} \|e\| = 0$, and hence the MMCCS between the two drive systems (27) and the two response systems (28) can be done. $\square$

3. Special cases

In this section, we introduce three examples to test the validity of our theorems of Section 2 and the control functions to achieve these kinds of modulus–modulus synchronization.

3.1. CMMS for chaotic complex Chen and Lorenz systems

In this example, we consider the complex Chen system (1) as the drive system and the complex Lorenz system (2) as the response one to achieve the CMMS. The response system after adding the control functions takes the form of

$$\begin{aligned} \dot{y_1} &= \sigma(y_2 - y_1) + u_1\,, \\ \dot{y_2} &= cy_1 - y_1y_3 - ay_2 + u_2\,, \\ \dot{y_3} &= \tfrac{1}{2}\left(\bar{y}_1y_2 + \bar{y}_2y_1\right) - by_3 + u_3\,, \end{aligned} \tag{38}$$

where u_1, u_2, u_3 are the control functions

$$\begin{aligned} f(x) &= \begin{pmatrix} a_1(x_2 - x_1) \\ (a_2 - a_1)x_1 - x_1x_3 + a_2x_2 \\ \frac{1}{2}\left(\bar{x}_1x_2 + \bar{x}_2x_1\right) - a_3x_3 \end{pmatrix} \\ &= f^r(x) + jf^i(x) = \begin{pmatrix} a_1\left(x_2^r - x_1^r\right) \\ (a_2 - a_1)x_1^r - x_1^rx_3^r + a_2x_2^r \\ \left(x_1^rx_2^r + x_1^ix_2^i\right) - a_3x_3^r \end{pmatrix} \\ &\quad + j\begin{pmatrix} a_1\left(x_2^i - x_1^i\right) \\ (a_2 - a_1)x_1^i - x_1^ix_3^i + a_2x_2^i \\ 0 \end{pmatrix}, \end{aligned} \tag{39}$$

and

$$\begin{aligned} g(y) &= \begin{pmatrix} \sigma(y_2 - y_1) \\ cy_1 - y_1y_3 - ay_2 \\ \frac{1}{2}\left(\bar{y}_1y_2 + \bar{y}_2y_1\right) - by_3 \end{pmatrix} = g^r(y) + jg^i(y) \\ &= \begin{pmatrix} \sigma\left(y_2^r - y_1^r\right) \\ cy_1^r - y_1^ry_3^r - ay_2^r \\ \left(y_1^ry_2^r + y_1^iy_2^i\right) - by_3^r \end{pmatrix} + j\begin{pmatrix} \sigma\left(y_2^i - y_1^i\right) \\ cy_1^i - y_1^iy_3^i - ay_2^i \\ 0 \end{pmatrix}. \end{aligned} \tag{40}$$

Applying Theorem 2.3, the control functions (9) and (10) are

$$\begin{pmatrix} u_1^r \\ u_2^r \\ u_3^r \end{pmatrix} = \begin{pmatrix} -\sigma\left(y_2^r - y_1^r\right) + \frac{x_1^r}{y_1^r}\frac{\sqrt{\left(y_1^r\right)^2+\left(y_1^i\right)^2}}{\sqrt{\left(x_1^r\right)^2+\left(x_1^i\right)^2}}\left(a_1\left(x_2^r - x_1^r\right)\right) - \frac{\sqrt{\left(y_1^r\right)^2+\left(y_1^i\right)^2}}{y_1^r}e_1 \\ -cy_1^r + y_1^r y_3^r + ay_2^r + \frac{x_2^r}{y_2^r}\frac{\sqrt{\left(y_2^r\right)^2+\left(y_2^i\right)^2}}{\sqrt{\left(x_2^r\right)^2+\left(x_2^i\right)^2}}\left(\left(a_2 - a_1\right)x_1^r - x_1^r x_3^r + a_2 x_2^r\right) - 2\frac{\sqrt{\left(y_2^r\right)^2+\left(y_2^i\right)^2}}{y_2^r}e_2 \\ -y_1^r y_2^r + by_3^r + \frac{x_3^r}{y_3^r}\frac{\sqrt{\left(y_3^r\right)^2+\left(y_3^i\right)^2}}{\sqrt{\left(x_3^r\right)^2+\left(x_3^i\right)^2}}\left(x_1^r x_2^r - a_3 x_3^r\right) - 3\frac{\sqrt{\left(y_3^r\right)^2+\left(y_3^i\right)^2}}{y_3^r}e_3 \end{pmatrix} \tag{41}$$

and

$$\begin{pmatrix} u_1^i \\ u_2^i \\ u_3^i \end{pmatrix} = \begin{pmatrix} -\sigma\left(y_2^i - y_1^i\right) + \frac{x_1^i}{y_1^i}\frac{\sqrt{\left(y_1^r\right)^2+\left(y_1^i\right)^2}}{\sqrt{\left(x_1^r\right)^2+\left(x_1^i\right)^2}}\left(a_1\left(x_2^i - x_1^i\right)\right) \\ -cy_1^i + y_1^i y_3^i + ay_2^i + \frac{x_2^i}{y_2^i}\frac{\sqrt{\left(y_2^r\right)^2+\left(y_2^i\right)^2}}{\sqrt{\left(x_2^r\right)^2+\left(x_2^i\right)^2}}\left(\left(a_2 - a_1\right)x_1^i - x_1^i x_3^i + a_2 x_2^i\right) \\ -y_1^i y_2^i + \frac{x_3^i}{y_3^i}\frac{\sqrt{\left(y_3^r\right)^2+\left(y_3^i\right)^2}}{\sqrt{\left(x_3^r\right)^2+\left(x_3^i\right)^2}}\left(x_1^i x_2^i\right) \end{pmatrix}, \tag{42}$$

where,

$$\begin{aligned} e_1 &= |y_1| - |x_1| = \sqrt{\left(y_1^r\right)^2 + \left(y_1^i\right)^2} - \sqrt{\left(x_1^r\right)^2 + \left(x_1^i\right)^2}, \\ e_2 &= |y_2| - |x_2| = \sqrt{\left(y_2^r\right)^2 + \left(y_2^i\right)^2} - \sqrt{\left(x_2^r\right)^2 + \left(x_2^i\right)^2}, \\ e_3 &= |y_3| - |x_3| = \sqrt{\left(y_3^r\right)^2 + \left(y_3^i\right)^2} - \sqrt{\left(x_3^r\right)^2 + \left(x_3^i\right)^2}. \end{aligned} \tag{43}$$

The error system (13) is constructed by combining the control functions (41) and (42) as

$$\dot{e} = \begin{pmatrix} \dot{e}_1 \\ \dot{e}_2 \\ \dot{e}_3 \end{pmatrix} = -K_1 e = -\mathrm{diag}(1,2,3)e = -\begin{pmatrix} 1 & 0 & 0 \\ 0 & 2 & 0 \\ 0 & 0 & 3 \end{pmatrix} e\,. \tag{44}$$

By using the method of Runge–Kutta of the order of 4, we solve numerically the response system (38) and the drive system (1) with the control functions (41)–(42). The initial conditions of system (1) and system (38) are, respectively, $(x_1, x_2, x_3)^{\mathrm{T}}(0) = (0.1+0.2j, 0.3+0.4j, 0.5)^{\mathrm{T}}$, $(y_1, y_2, y_3)^{\mathrm{T}}(0) =$

$(0.2+0.4j, 0.6+0.8j, 1)^{\mathrm{T}}$, and the values of these systems parameters are: $a_1 = 35$, $a_2 = 28$, $a_3 = 3$, $\sigma = 2$, $c = 60 + 0.02j$, $a = 1 - 0.06j$, $b = 0.8$. Figures 1–2 illustrate the CMMS results between systems (1) and (38). Figure 1 shows a 3D projection of the solution of the drive system (1) and the response one (38). In addition, the synchronization errors e_i $(i = 1, 2, 3)$, as shown in Fig. 2, go to zero.

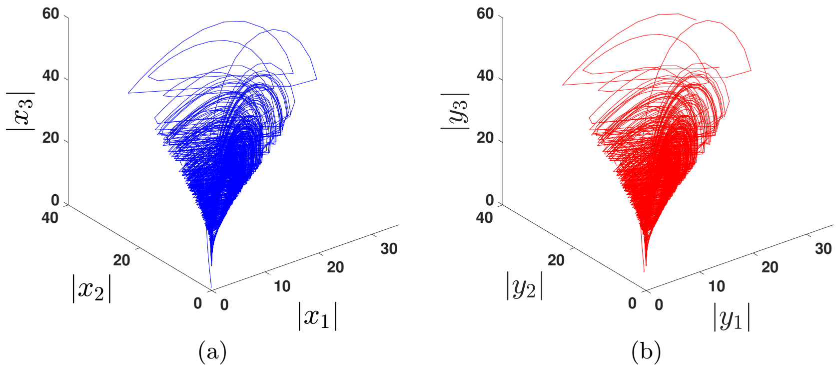

Fig. 1. CMMS of: (a) the drive system (1) in $(|x_1|, |x_2|, |x_3|)$ space and (b) the response system (38) in $(|y_1|, |y_2|, |y_3|)$ space.

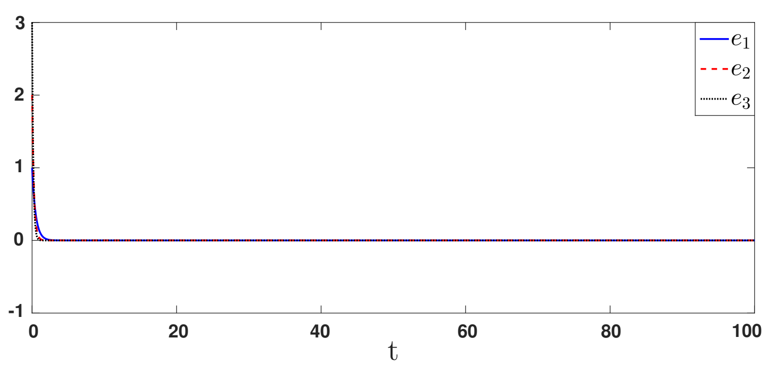

Fig. 2. Synchronization errors for the drive system (1) and the response system (38).

3.2. MMCS between three chaotic complex systems

To achieve the MMCS, we consider the Chen (1) and Lorenz (2) systems as two drive systems, and the Lü system (3) as the response one. After adding the control functions, the response system is

$$\begin{aligned}
\dot{z}_1 &= c_1(z_2 - z_1) + u_1\,, \\
\dot{z}_2 &= -z_1 z_3 + c_2 z_2 + u_2\,, \\
\dot{z}_3 &= \tfrac{1}{2}(\bar{z}_1 z_2 + \bar{z}_2 z_1) - c_3 z_3 + u_3\,,
\end{aligned} \tag{45}$$

where u_1, u_2, u_3 are the control functions and $f(x)$, $g(y)$ defined in Subsection 3.1, and $h(z)$ is

$$\begin{aligned}
h(z) &= \begin{pmatrix} c_1(z_2 - z_1) \\ -z_1 z_3 + c_2 z_2 \\ \frac{1}{2}\left(\bar{z}_1 z_2 + \bar{z}_2 z_1\right) - c_3 z_3 \end{pmatrix} \\
&= h^r(z) + j h^i(z) = \begin{pmatrix} c_1\left(z_2^r - z_1^r\right) \\ -z_1^r z_3^r + c_2 z_2^r \\ \left(z_1^r z_2^r + z_1^i z_2^i\right) - c_3 z_3^r \end{pmatrix} \\
&\quad + j \begin{pmatrix} c_1\left(z_2^i - z_1^i\right) \\ -z_1^i z_3^i + c_2 z_2^i \\ 0 \end{pmatrix}.
\end{aligned} \tag{46}$$

Using Theorem 2.6, the control functions (20) and (21) become

$$\begin{pmatrix} u_1^r \\ u_2^r \\ u_3^r \end{pmatrix} = \begin{pmatrix}
-c_1\left(z_2^r - z_1^r\right) + \frac{x_1^r + y_1^r}{z_1^r} \frac{\sqrt{\left(z_1^r\right)^2 + \left(z_1^i\right)^2}}{\sqrt{\left(x_1^r + y_1^r\right)^2 + \left(x_1^i + y_1^i\right)^2}} \\
\times \left(a_1\left(x_2^r - x_1^r\right) + \sigma\left(y_2^r - y_1^r\right)\right) - \frac{\sqrt{\left(z_1^r\right)^2 + \left(z_1^i\right)^2}}{z_1^r} e_1 \\
\\
z_1^r z_3^r - c_2 z_2^r + \frac{x_2^r + y_2^r}{z_2^r} \frac{\sqrt{\left(z_2^r\right)^2 + \left(z_2^i\right)^2}}{\sqrt{\left(x_2^r + y_2^r\right)^2 + \left(x_2^i + y_2^i\right)^2}} \\
\times \left(\left(a_2 - a_1\right) x_1^r - x_1^r x_3^r + a_2 x_2^r + c y_1^r - y_1^r y_3^r - a y_2^r\right) - 3 \frac{\sqrt{\left(z_2^r\right)^2 + \left(z_2^i\right)^2}}{z_2^r} e_2 \\
\\
-z_1^r z_2^r + c_3 z_3^r + \frac{x_3^r + y_3^r}{z_3^r} \frac{\sqrt{\left(z_3^r\right)^2 + \left(z_3^i\right)^2}}{\sqrt{\left(x_3^r + y_3^r\right)^2 + \left(x_3^i + y_3^i\right)^2}} \\
\times \left(x_1^r x_2^r - a_3 x_3^r + y_1^r y_2^r - b y_3^r\right) - 5 \frac{\sqrt{\left(z_3^r\right)^2 + \left(z_3^i\right)^2}}{z_3^r} e_3
\end{pmatrix} \tag{47}$$

and

$$\begin{pmatrix} u_1^i \\ \\ u_2^i \\ \\ u_3^i \end{pmatrix} = \left(\begin{array}{l} -c_1\left(z_2^i - z_1^i\right) + \frac{x_1^i+y_1^i}{z_1^i} \frac{\sqrt{\left(z_1^r\right)^2+\left(z_1^i\right)^2}}{\sqrt{\left(x_1^r+y_1^r\right)^2+\left(x_1^i+y_1^i\right)^1}} \\ \times \left(a_1\left(x_2^i - x_1^i\right) + \sigma\left(y_2^i - y_1^i\right)\right) \\ \\ z_1^i z_3^i - c_2 z_2^i + \frac{x_2^i+y_2^i}{z_2^i} \frac{\sqrt{\left(z_2^r\right)^2+\left(z_2^i\right)^2}}{\sqrt{\left(x_2^r+y_2^r\right)^2+\left(x_2^i+y_2^i\right)^2}} \\ \times \left(\left(a_2 - a_1\right) x_1^i - x_1^i x_3^i + a_2 x_2^i + c y_1^i - y_1^i y_3^i - a y_2^i\right) \\ \\ -z_1^i z_2^i + \frac{x_3^i+y_3^i}{z_3^i} \frac{\sqrt{\left(z_3^r\right)^2+\left(z_3^i\right)^2}}{\sqrt{\left(x_3^r+y_3^r\right)^2+\left(x_3^i+y_3^i\right)^2}} \left(x_1^i x_2^i + y_1^i y_2^i\right) \end{array} \right), \tag{48}$$

where

$$\begin{aligned} e_1 &= |z_1| - |x_1+y_1| = \sqrt{\left(z_1^r\right)^2 + \left(z_1^i\right)^2} - \sqrt{\left(x_1^r + y_1^r\right)^2 + \left(x_1^i + y_1^i\right)^2}, \\ e_2 &= |z_2| - |x_2+y_2| = \sqrt{\left(z_2^r\right)^2 + \left(z_2^i\right)^2} - \sqrt{\left(x_2^r + y_2^r\right)^2 + \left(x_2^i + y_2^i\right)^2}, \\ e_3 &= |z_3| - |x_3+y_3| = \sqrt{\left(z_3^r\right)^2 + \left(z_3^i\right)^2} - \sqrt{\left(x_3^r + y_3^r\right)^2 + \left(x_3^i + y_3^i\right)^2}. \end{aligned} \tag{49}$$

Using the control functions (47) and (48), the error system (24) can be represented as

$$\dot{e} = \begin{pmatrix} \dot{e}_1 \\ \dot{e}_2 \\ \dot{e}_3 \end{pmatrix} = -K_2 e = -\mathrm{diag}(1,3,5)e = -\begin{pmatrix} 1 & 0 & 0 \\ 0 & 3 & 0 \\ 0 & 0 & 5 \end{pmatrix} e\,. \tag{50}$$

The response system (45) and the drive systems (1) and (2) are solved numerically with the control functions (47)–(48). The initial conditions of systems (1), (2), and (45) are, respectively, $(x_1, x_2, x_3)^{\mathrm{T}}(0) = (0.1 + 0.2j, 0.3 + 0.4j, 0.5)^{\mathrm{T}}$, $(y_1, y_2, y_3)^{\mathrm{T}}(0) = (0.2 + 0.4j, 0.6 + 0.8j, 1)^{\mathrm{T}}$, $(z_1, z_2, z_3)^{\mathrm{T}}(0) = (0.1 + 0.2j, 0.3 + 0.4j, 0.5)^{\mathrm{T}}$, and the values of parameters of these systems are: $a_1 = 35$, $a_2 = 28$, $a_3 = 3$, $\sigma = 2$, $c = 60 + j0.02$, $a = 1 - 0.06j$, $b = 0.8$, $c_1 = 36$, $c_2 = 20$, $c_3 = 3$. Figures 3–4 indicate the results of MMCS between the systems (1), (2), and (45). Figure 3 presents the state variables of the drive systems (1) and (2), and the response system (45). Furthermore, as shown in Fig. 4, the synchronization errors e_i $(i = 1, 2, 3)$ approach zero.

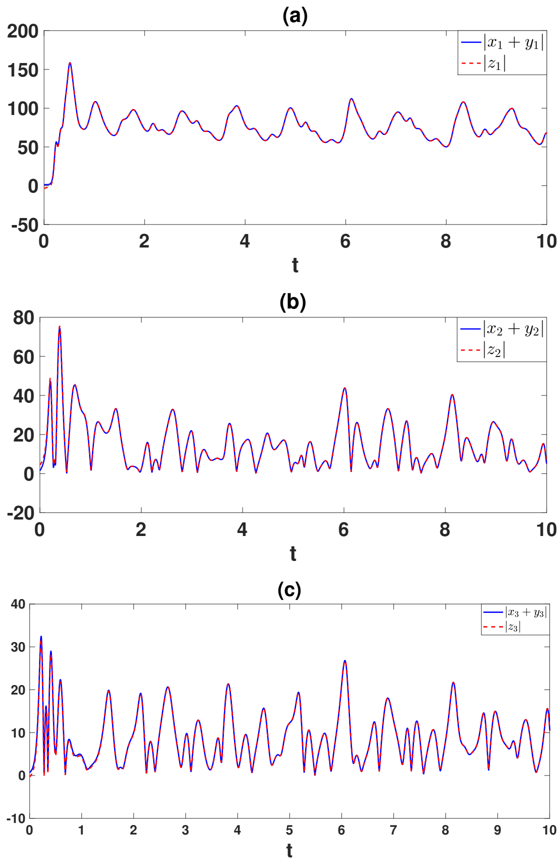

Fig. 3. The state variables for MMCS for the two drive systems (1),(2) (solid curves) and the response system (45) (dashed curves): (a) $|x_1 + y_1|$ and $|z_1|$ *versus* t, (b) $|x_2 + y_2|$ and $|z_2|$ *versus* t, and (c) $|x_3 + y_3|$ and $|z_3|$ *versus* t.

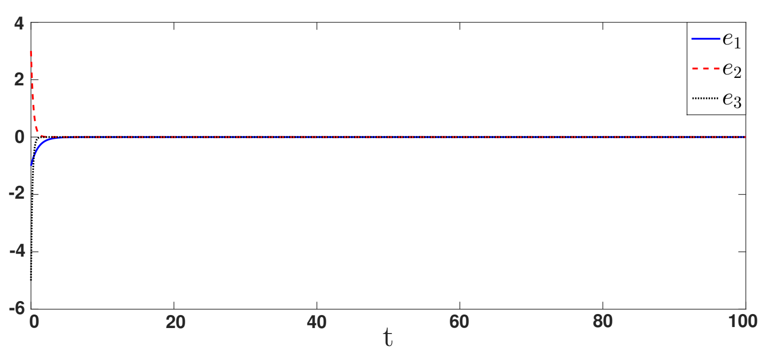

Fig. 4. Synchronization errors for the drive systems (1)–(2) and the response system (45).

3.3. MMCCS between four chaotic complex systems

To achieve the MMCCS, we consider the Chen and Lorenz systems (1) and (2) as two drive systems, and the Lü and Rössler systems (3) and (4) as the response systems. The two response systems after adding the control functions take the form of

$$\begin{aligned}
\dot{z_1} &= c_1(z_2 - z_1) + u_1 \,, \\
\dot{z_2} &= -z_1 z_3 + c_2 z_2 + u_2 \,, \\
\dot{z_3} &= \tfrac{1}{2}\left(\bar{z}_1 z_2 + \bar{z}_2 z_1\right) - c_3 z_3 + u_3
\end{aligned} \tag{51}$$

and

$$\begin{aligned}
\dot{w_1} &= -w_1 - w_3 + v_1 \,, \\
\dot{w_2} &= w_1 + d_1 w_2 + v_2 \,, \\
\dot{w_3} &= d_2 + \tfrac{1}{2} w_3 \left(w_1 + \bar{w}_1 - 2d_3\right) + v_3 \,,
\end{aligned} \tag{52}$$

where $u_1, u_2, u_3, v_1, v_2, v_3$ are the control functions and $f(x)$, $g(y)$, and $h(z)$ are defined in Subsection 3.1–3.2 and $s(w)$ is

$$\begin{aligned}
s(w) &= \begin{pmatrix} -w_2 - w_3 \\ w_1 + d_1 w_2 \\ d_2 + \frac{1}{2} w_3 \left(w_1 + \bar{w}_1 - 2d_3\right) \end{pmatrix} \\
&= s^r(w) + j s^r(w) = \begin{pmatrix} -w_2^r - w_3^r \\ w_1^r + d_1 w_2^r \\ d_2 + w_3^r \left(w_1^r - d_3\right) \end{pmatrix} \\
&\quad + j \begin{pmatrix} -w_2^i - w_3^i \\ w_1^i + d_1 w_2^i \\ 0 \end{pmatrix} .
\end{aligned} \tag{53}$$

Using Theorem 2.9, the control functions (31) and (32) are

$$\begin{pmatrix} u_1^r + v_1^r \\ u_2^r + v_2^r \\ u_3^r + v_3^r \end{pmatrix}$$

$$= \begin{pmatrix} \left(-c_1\left(z_2^r - z_1^r\right) + w_2^r + w_3^r\right) + \frac{x_1^r + y_1^r}{z_1^r + w_1^r} \frac{\sqrt{\left(z_1^r + w_1^r\right)^2 + \left(z_1^i + w_1^i\right)^2}}{\sqrt{\left(x_1^r + y_1^r\right)^2 + \left(x_1^i + y_1^i\right)^2}} \\ \times \left(a_1\left(x_2^r - x_1^r\right) + \sigma\left(y_2^r - y_1^r\right)\right) \\ \\ \left(z_1^r z_3^r - c_2 z_2^r - w_1^r - d_1 w_2^r\right) + \frac{x_2^r + y_2^r}{z_2^r + w_2^r} \frac{\sqrt{\left(z_2^r + w_2^r\right)^2 + \left(z_2^i + w_2^i\right)^2}}{\sqrt{\left(x_2^r + y_2^r\right)^2 + \left(x_2^i + y_2^i\right)^2}} \\ \times \left((a_2 - a_1)x_1^r - x_1^r x_3^r + a_2 x_2^r + c y_1^r - y_1^r y_3^r - a y_2^r\right) \\ \\ \left(-z_1^r z_2^r + c_3 z_3^r - d_2 - w_3^r\left(w_1^r - d_3\right)\right) + \frac{x_3^r + y_3^r}{z_3^r + w_3^r} \frac{\sqrt{\left(z_3^r + w_3^r\right)^2 + \left(z_3^i + w_3^i\right)^2}}{\sqrt{\left(x_3^r + y_3^r\right)^2 + \left(x_3^i + y_3^i\right)^2}} \\ \times \left(x_1^r x_2^r - a_3 x_3^r + y_1^r y_2^r - b y_3^r\right) \end{pmatrix}$$

$$- \begin{pmatrix} 4 \frac{\sqrt{\left(z_1^r + w_1^r\right)^2 + \left(z_1^i + w_1^i\right)^2}}{z_1^r + w_1^r} e_1 \\ 3 \frac{\sqrt{\left(z_2^r + w_2^r\right)^2 + \left(z_2^i + w_2^1\right)^2}}{z_2^r + w_2^r} e_2 \\ 7 \frac{\sqrt{\left(z_3^r + w_3^r\right)^2 + \left(z_3^i + w_3^1\right)^2}}{z_3^r + w_3^r} e_3 \end{pmatrix} \tag{54}$$

and

$$\begin{pmatrix} u_1^i + v_1^i \\ u_2^i + v_2^i \\ u_3^i + v_2^i \end{pmatrix} = \begin{pmatrix} \left(-c_1\left(z_2^i - z_1^i\right) + w_2^i + w_3^i\right) + \frac{x_1^i+y_1^i}{z_1^i+w_1^i}\frac{\sqrt{\left(z_1^r+w_1^r\right)^2+\left(z_1^i+w_1^i\right)^2}}{\sqrt{\left(x_1^r+y_1^r\right)^2+\left(x_1^i+y_1^i\right)^2}} \\ \times\left(a_1\left(x_2^i - x_1^i\right) + \sigma\left(y_2^i - y_1^i\right)\right) \\ \\ \left(z_1^i z_3^i - c_2 z_2^i - w_1^i - d_1 w_2^i\right) + \frac{x_2^i+y_2^i}{z_2^i+w_2^i}\frac{\sqrt{\left(z_2^r+w_2^r\right)^2+\left(z_2^i+w_2^i\right)^2}}{\sqrt{\left(x_2^r+y_2^r\right)^2+\left(x_2^i+y_2^i\right)^2}} \\ \times\left((a_2-a_1)x_1^i - x_1^i x_3^i + a_2 x_2^i + c y_1^i - y_1^i y_3^i - a y_2^i\right) \\ \\ \left(-z_1^i z_2^i + c_3 z_3^i - d_2 - w_3^i\left(w_1^i - d_3\right)\right) + \frac{x_3^i+y_3^i}{z_3^i+w_3^i}\frac{\sqrt{\left(z_3^r+w_3^r\right)^2+\left(z_3^i+w_3^i\right)^2}}{\sqrt{\left(x_3^r+y_3^r\right)^2+\left(x_3^i+y_3^i\right)^2}} \\ \times\left(x_1^i x_2^i - a_3 x_3^i + y_1^i y_2^i - b y_3^i\right) \end{pmatrix}, \tag{55}$$

where

$$\begin{aligned} e_1 &= |z_1 + w_1| - |x_1 + y_1| \\ &= \sqrt{\left(z_1^r + w_1^r\right)^2 + \left(z_1^i + w_1^i\right)^2} - \sqrt{\left(x_1^r + y_1^r\right)^2 + \left(x_1^i + y_1^i\right)^2}, \\ e_2 &= |z_2 + w_2| - |x_2 + y_2| \\ &= \sqrt{\left(z_2^r + w_2^r\right)^2 + \left(z_2^i + w_2^i\right)^2} - \sqrt{\left(x_2^r + y_2^r\right)^2 + \left(x_2^i + y_2^i\right)^2}, \\ e_3 &= |z_3 + w_3| - |x_3 + y_3| \\ &= \sqrt{\left(z_3^r + w_3^r\right)^2 + \left(z_3^i + w_3^i\right)^2} - \sqrt{\left(x_3^r + y_3^r\right)^2 + \left(x_3^i + y_3^i\right)^2}. \end{aligned} \tag{56}$$

Using the control functions (54) and (55), the error system (35) for this example is

$$\dot{e} = \begin{pmatrix} \dot{e}_1 \\ \dot{e}_2 \\ \dot{e}_3 \end{pmatrix} = -K_3 e = -\mathrm{diag}(4,3,7)e = -\begin{pmatrix} 4 & 0 & 0 \\ 0 & 3 & 0 \\ 0 & 0 & 7 \end{pmatrix} e\,. \tag{57}$$

The two drive and two response systems (1), (2), (51), and (52) are solved numerically with the control functions (54)–(55). The initial conditions of the systems (1), (2), (51), and (52) are, respectively, $(x_1, x_2, x_3)^{\mathrm{T}}(0) = (0.1 + 0.2j, 0.3 + 0.4j, 0.5)^{\mathrm{T}}$, $(y_1, y_2, y_3)^{\mathrm{T}}(0) = (0.2 + 0.4j, 0.6 + 0.8j, 1)^{\mathrm{T}}$, $(z_1, z_2, z_3)^{\mathrm{T}}(0) = (0.1 + 0.2j, 0.3 + 0.4j, 0.5)^{\mathrm{T}}$, $(w_1, w_2, w_3)^{\mathrm{T}}(0) = (0.2 + 0.4j, 0.6 + 0.8j, 1)^{\mathrm{T}}$, and these systems parameters are: $a_1 = 35$, $a_2 = 28$, $a_3 = 3$, $\sigma = 2$, $c = 60 + j0.02$, $a = 1 - j0.06$, $b = 0.8$, $c_1 = 36$, $c_2 = 20$, $c_3 = 3$, $d_1 = 0.2$, $d_2 = 0.2$, $d_3 = 5.7$. The results of MMCCS among systems (1), (2), (51), and (52) are displayed in Figs. 5–6. Figure 5, describes the 3D projection of the solution of the drive and response systems after synchronization. Also, the synchronization errors go to zero as depicted in Fig. 6.

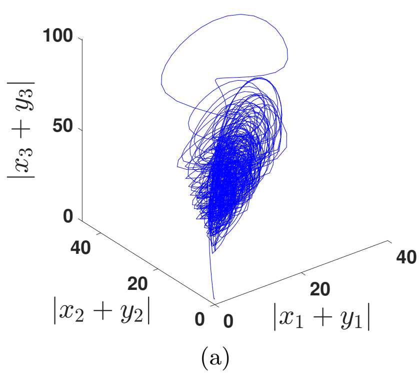

Fig. 5. MMCCS of: (a) the drive systems (1)–(2) in $(|x_1 + y_1|, |x_2 + y_2|, |x_3 + y_3|)$ space and (b) the response systems (51)–(52) in $(|z_1 + w_1|, |z_2 + w_2|, |z_3 + w_3|)$ space.

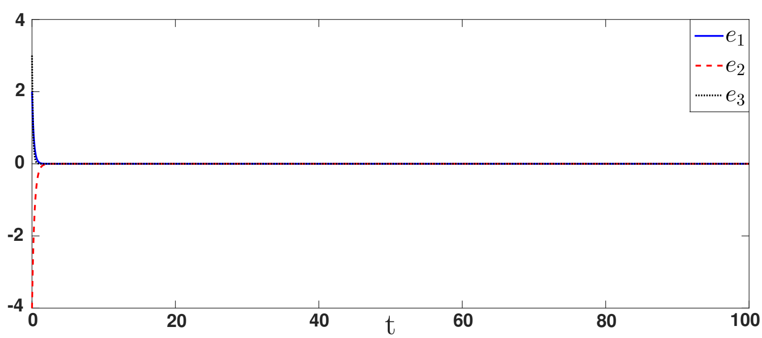

Fig. 6. Synchronization errors for the drive systems (1)–(2) and the response systems (51)–(52).

4. Application to image encryption

In this section, we investigate the application of image encryption based on the CMMS between chaotic complex Chen and Lorenz systems. In the sender, we consider the complex Chen (1) as the drive system that generates chaotic signals (sequence); then signals will drive the response system (38) to achieve synchronization with the drive system (1).

4.1. Encryption process

The steps for the encryption process to the application of image encryption are described as follows:

Step 1: The original grayscale image, P, of the size $M \times N$ is represented as $M \times N$ matrix of pixels as follows:

$$P = \begin{pmatrix} p_{11} & p_{12} & \cdots & p_{1N} \\ \vdots & \vdots & \ddots & \vdots \\ p_{M1} & p_{M2} & \cdots & p_{MN} \end{pmatrix} . \tag{58}$$

Step 2: The $2D$ matrix, P, is converted to $1D$ matrix (vector), E, with the length $M \times N$, which is defined as

$$\begin{aligned} E &= [p_{11}, p_{12}, \ldots, p_{1N}, p_{21}, p_{22}, \ldots, p_{2N}, p_{M1}, p_{M2}, \ldots, p_{MN}] \\ &= [B_1, B_2, \ldots, B_{MN}] . \end{aligned} \tag{59}$$

Each element in vector E is an integer from 0 to 255.

Step 3: Suppose that the synchronization is achieved between the drive system (1) and the response system (38).

Step 4: The chaotic sequence can be produced from the chaotic drive system (1). Iterate the system (38) for $N_0 + M \times N$ times and discard the former N_0 values, a chaotic decimal sequence, S, with the length $M \times N$ can be produced as follows:

$$S = [S_1, S_2, \ldots, S_{MN}] . \tag{60}$$

Step 5: The decimal chaotic sequence, S, is sorted in the ascending order.

Step 6: According to step 5, the decimal values, K, can be computed as follows:

$$K = \mathrm{mod}\left(\mathrm{floor}(S) \times 10^8, 256\right) , \tag{61}$$

where floor(m) rounds m to the nearest integer less than or equal to m and mod(a, b) returns the remainder after division $\frac{a}{b}$.

Step 7: The encrypted (cipher) vector H is produced as follows:

$$H = K \oplus E\,, \tag{62}$$

where $\oplus$ the exclusive XOR operation.

Step 8: The encrypted image vector H is transformed into $2D$ matrix to produce the encrypted image with the size $M \times N$.

Remark 4.1. A similar encryption process can be designed for MMCS using the drive systems (1) and (2), and the response system (45). The same can be done for MMCCS based on the drive systems (3) and (4) and the response systems (51) and (52).

4.2. Decryption process

As we know, the decryption is the reverse process of encryption and the key used for encryption and decryption are the same. The generated chaotic sequence is consistent for the encryption and decryption process. Therefore, the encryption application is symmetric and reversible, and we can easily decrypt the encrypted image with the inverse steps of the encryption process.

4.3. Experimental results

We conducted numerous experiments on different standard grayscale images of the size 512×512 (Lake, Pirate, Barbara, and Boat) to validate the application's security and effectiveness. The original grayscale images (Pirate, Barbara, and Boat), the encrypted images and the corresponding decrypted images based on CMMS are shown in Fig. 7, respectively. According to Fig. 7, the plaintext image's visual information cannot be seen in the ciphertext image, and the restored ciphertext images and plaintext images have no significant differences. As a result, the application encryption could be used to effectively hide image information. In the decryption algorithm, the parameter and initial values are the same as the encryption algorithm.

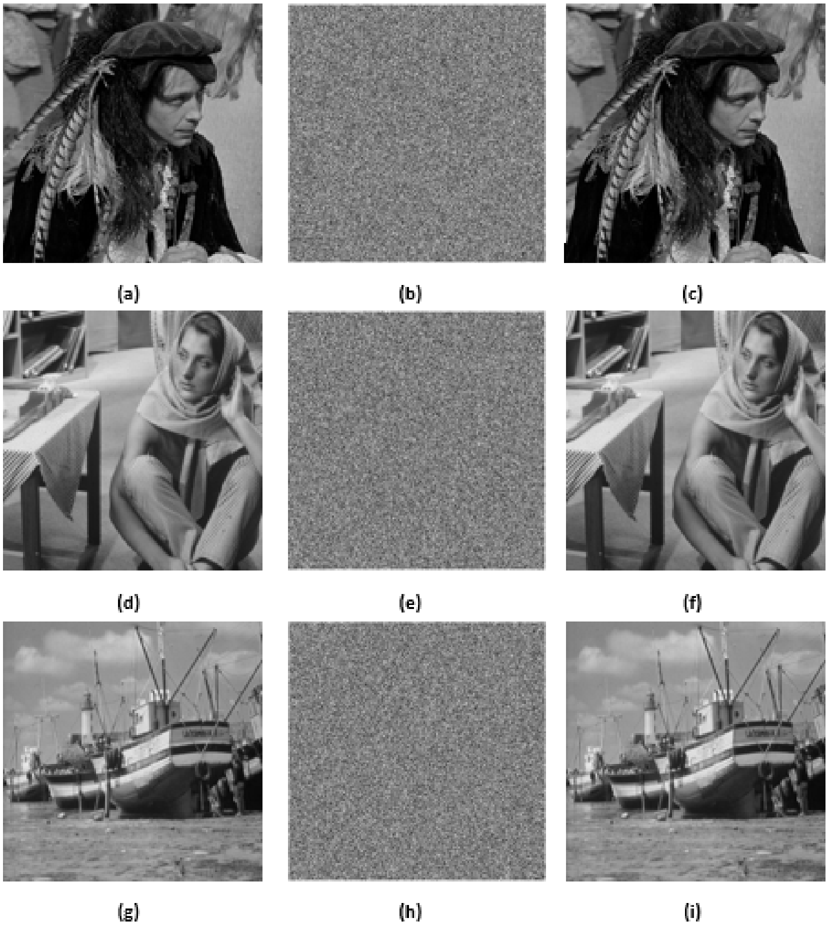

Fig. 7. Image encryption/decryption experiment results of images with a size of 512×512: (a) Image Pirate, (b) Ciphered image of (a), (c) Decrypted image of (b), (d) Image Barbara, (e) Ciphered image of (d), (f) Decrypted image of (e), (g) Image Boat, (h) Ciphered image of (g), and (i) Decrypted image of (h).

4.3.1. Information entropy

Information entropy is used to measure the randomness of an image, which is calculated as follows:

$$H(x) = \sum_{i=1}^{N} p(x_i) \log_2 \frac{1}{p(x_i)}\,, \tag{63}$$

where N denotes the number of gray levels, x_i denotes the pixel value of the image, and $p(x_i)$ denotes the frequency of the gray level.

The stronger randomness is the higher entropy. It is generally accepted that the ideal information entropy for 256 grayscale images is 8. When the information entropy approaches 8, the cipher image becomes more confusing and secure. In order to evaluate the encryption procedure, four images are examined for the information entropy. The test results are provided in Table 1. It can be seen that all encrypted images obtained by the encryption process in this paper are close to 8, which significantly improves the image's information entropy. It is clear that the information entropy is approaching the ideal value.

Table 1. The information entropy of plain images and their corresponding encrypted images.

Image		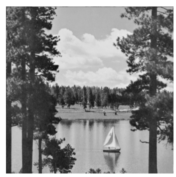		
Plain images	7.450367	7.518523	7.32549	7.59481
Encrypted images	7.999856	7.999376	7.998854	7.99947

4.3.2. Correlation analysis of adjacent pixels

The correlation coefficient of two pixels denotes the degree of correlation between two pixels. There is a strong correlation between adjacent pixels in the horizontal, vertical, and diagonal directions of the plaintext, whereas there is no correlation between adjacent pixels in the effectively encrypted image. The image's adjacent pixel correlation coefficient is calculated as follows:

$$r_{x,y} = \frac{\operatorname{cov}(x,y)}{\sqrt{D(y)D(x)}}, \tag{64}$$

$$\operatorname{cov}(x,y) = E((x-E(x))(y-E(y))), \tag{65}$$

$$E(x) = \frac{1}{N}\sum_{i=1}^{N} x_i, \tag{66}$$

$$D(x) = \frac{1}{N}\sum_{i=1}^{N}(x_i - E(x))^2, \tag{67}$$

where x and y are the gray values of two adjacent pixels. $\mathrm{cov}(x, y)$, $D(x)$, and $E(x)$ are covariance, variance, and expectation, respectively. Ideally, the correlation between adjacent pixels in a successful encrypted image should be close to zero.

The correlation coefficients in the horizontal, vertical, and diagonal directions are calculated by randomly selecting 2000 pixels in plaintext image and ciphertext image and, calculating the correlation coefficients in those directions. The correlation test results of 4 grayscale images are listed in Table 2. It can be seen that all the horizontal, vertical, and diagonal correlations between adjacent pixels of the original image are very close to 1. A ciphertext image, on the other hand, has a correlation coefficient that is close to 0. As a result, the scheme is able to eliminate the correlation between adjacent pixels and could undergo statistical attacks.

Table 2. Correlation coefficients between adjacent pixels of images.

Image	Direction	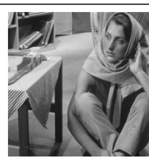	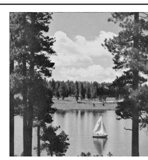		
Plain images	Horizontal	0.9285	0.9758	0.9467	0.9657
	Vertical	0.9352	0.9883	0.9548	0.9832
	Diagonal	0.9387	0.9646	0.9389	0.9685
Encrypted images	Horizontal	0.0049	0.0031	0.0043	0.0038
	Vertical	0.0038	0.0038	0.0011	0.0054
	Diagonal	0.0069	0.0020	0.0024	0.0030

4.3.3. Histogram analysis

A histogram is a statistical chart that represents the gray distribution of an image, and counts the occurrence times of each gray value. As long as the grayscale frequencies in the ciphered image are roughly equal, the histogram will be flat and resistant to statistical analysis attacks. The grayscale and encrypted images histograms are shown in Fig. 8. The pixel value distribution of the encrypted image is relatively uniform, as shown in Fig. 8, and the histograms of the ciphered images are nearly flat. Furthermore, the histogram of the encrypted images differs noticeably from that of the original image. As a result, the encryption scheme described in this paper can undergo statistical attacks. The results of this section based on CMMS can be similarly investigated but based on MMCS or MMCCS.

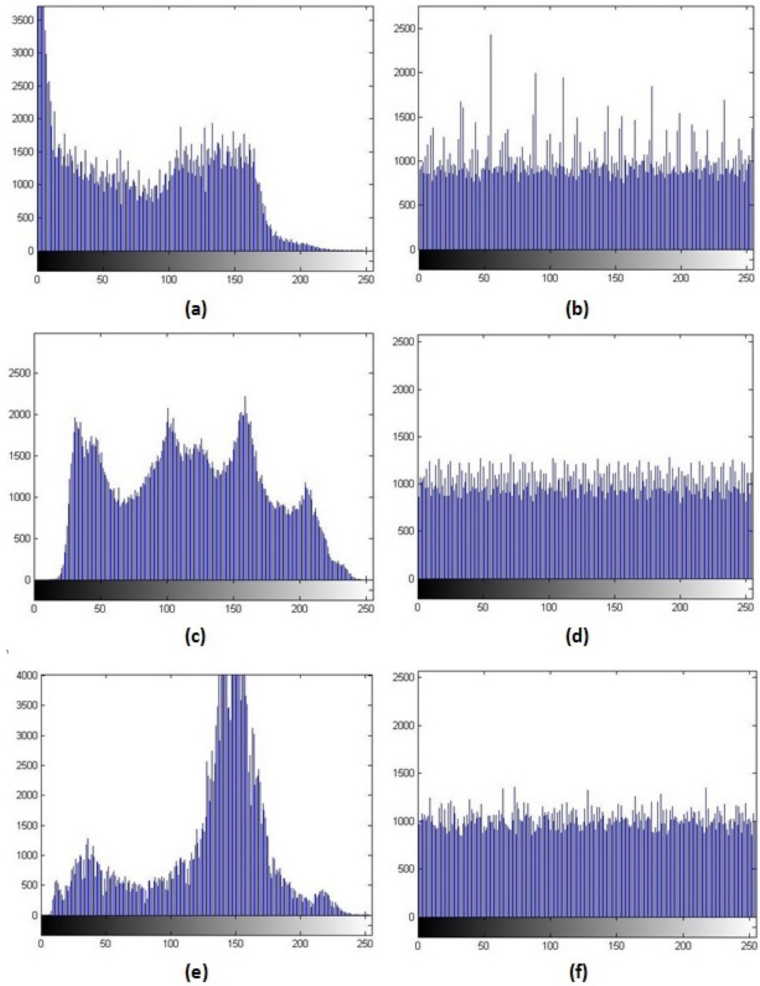

Fig. 8. Histogram plot of various plain images and their encrypted version. (a) plain Pirate, (b) encrypted Pirate, (c) plain Barbara, (d) encrypted Barbara, (e) plain Boat, (f) encrypted Boat.

5. Conclusions

Three new kinds of modulus–modulus synchronization between chaotic (or hyperchaotic) complex systems are proposed. These kinds are complete modulus–modulus synchronization (CMMS) between two systems, modulus–modulus combination synchronization (MMCS) between three systems, and modulus–modulus combination–combination synchronization (MMCCS) between four systems. The definitions of CMMS, MMCS, and MMCCS are considered as a generalization of those in the literature as stated in Remarks 2.2–2.8. Three theorems are introduced to provide us with analytical expressions of the control functions to achieve these kinds of synchronization. As special cases of these chaotic complex systems we choose Chen, Lorenz, Lü, and Rössler systems Eqs. (1), (2), (3), and (4), respectively. The corresponding analytical formulas of the control functions for CMMS, MMCS, and MMCCS are derived in Eqs. (41)–(42), (47)–(48), and (54)–(55), respectively. A good agreement is found between both analytical and numerical results as depicted in Figs. 1–6. The processes of encryption and decryption of images are stated based on CMMS between chaotic complex Chen and Lorenz in Subsection 4.1. The experimental results of images encryption and decryption using CMMS are shown in Fig. 7. The information entropy of our images is calculated and presented in Table 1. It is clear that they approach the ideal value which is 8. The grayscale and encrypted images histograms are shown in Fig. 8. The distributions of the encrypted images are relatively uniform and the histograms of the ciphered images are nearly flat. Figures 7–8 demonstrate that the encryption applications provide very high security performance and are more efficient. Similar investigations based on MMCS and MMCCS can be studied.

We are currently in the process of extending these investigations to other types of modulus–modulus synchronization in the near future, such as dual combination synchronization and double compound combination–combination synchronization. We will also consider these kinds of synchronization with time delay.

REFERENCES

[1] L.M. Pecora, T.L. Carroll, «Synchronization in chaotic systems», *Phys. Rev. Lett.* **64**, 821 (1990).

[2] C.-M. Kim *et al.*, «Anti-synchronization of chaotic oscillators», *Phys. Lett. A* **320**, 39 (2003).

[3] R. Mainieri, J. Rehacek, «Projective Synchronization In Three-Dimensional Chaotic Systems», *Phys. Rev. Lett.* **82**, 3042 (1999).

[4] G.-H. Li, «Modified projective synchronization of chaotic system», *Chaos Solitons Fract.* **32**, 1786 (2007).

[5] C. Li, X. Liao, K.-w. Wong, «Lag synchronization of hyperchaos with application to secure communications», *Chaos Solitons Fract.* **23**, 183 (2005).

[6] H. Du, Q. Zeng, C. Wang, «Function projective synchronization of different chaotic systems with uncertain parameters», *Phys. Lett. A* **372**, 5402 (2008).

[7] G.M. Mahmoud, M.E. Ahmed, T.M. Abed-Elhameed, «On fractional-order hyperchaotic complex systems and their generalized function projective combination synchronization», *Optik* **130**, 398 (2017).

[8] G.M. Mahmoud, T.M. Abed-Elhameed, H. Khalaf, «Synchronization of hyperchaotic dynamical systems with different dimensions», *Phys. Scr.* **96**, 125244 (2021).

[9] G.M. Mahmoud, T.M. Abed-Elhameed, M.E. Ahmed, «Generalization of combination–combination synchronization of chaotic n-dimensional fractional-order dynamical systems», *Nonlinear Dyn.* **83**, 1885 (2016).

[10] J. Sun *et al.*, «Compound-combination synchronization of five chaotic systems via nonlinear control», *Optik* **127**, 4136 (2016).

[11] G.M. Mahmoud, T.M. Abed-Elhameed, A.A. Farghaly, «Double compound combination synchronization among eight n-dimensional chaotic systems», *Chinese Phys. B* **27**, 080502 (2018).

[12] P. Li, J. Du, S. Li, Y. Zheng, «Modulus Synchronization of a Novel Hyperchaotic Real System and Its Corresponding Complex System», *IEEE Access* **7**, 109577 (2019).

[13] A. Khan, U. Nigar, «Modulus Synchronization in Non-identical Hyperchaotic Complex Systems and Hyperchaotic Real System Using Adaptive Control», *J. Contr. Autom. Electr. Syst.* **32**, 291 (2021).

[14] G.M. Mahmoud *et al.*, «Kinematic reconstructions of extended theories of gravity at small and intermediate redshifts», *Eur. Phys. J. Plus* **135**, 1 (2020).

[15] B. Nana, P. Woafo, S. Domngang, «Chaotic synchronization with experimental application to secure communications», *Commun. Nonlinear Sci. Numer. Simul.* **14**, 2266 (2009).

[16] H. Jahanshahi *et al.*, «A new fractional-order hyperchaotic memristor oscillator: Dynamic analysis, robust adaptive synchronization, and its application to voice encryption», *Appl. Math. Comput.* **383**, 125310 (2020).

[17] G.M. Mahmoud, A.A. Farghaly, T.M. Abed-Elhameed, M.M. Darwish, «Adaptive Dual Synchronization of Chaotic (Hyperchaotic) Complex Systems with Uncertain Parameters and Its Application in Image Encryption», *Acta Phys. Pol. B* **49**, 1923 (2018).

[18] A. Daneshgar, B. Khadem, «A self-synchronized chaotic image encryption scheme», *Signal Proces. Image Commun.* **36**, 106 (2015).

[19] Y. Xu, H. Wang, Y. Li, B. Pei, «Image encryption based on synchronization of fractional chaotic systems», *Commun. Nonlinear Sci. Numer. Simul.* **19**, 3735 (2014).

[20] W.S. Sayed, A.G. Radwan, «Generalized switched synchronization and dependent image encryption using dynamically rotating fractional-order chaotic systems», *AEU-Int. J. Electron. Commun.* **123**, 153268 (2020).

[21] S. Moon, J.-J. Baik, J.M. Seo, «Chaos synchronization in generalized Lorenz systems and an application to image encryption», *Commun. Nonlinear Sci. Numer. Simul.* **96**, 105708 (2021).

[22] G.M. Mahmoud, T. Bountis, E.E. Mahmoud, «Active Control and Global Synchronization of the Complex Chen and Lü Systems», *Int. J. Bifurcation Chaos* **17**, 4295 (2007).

[23] A. Fowler, J. Gibbon, M. McGuinness, «The complex Lorenz equations», *Physica D: Nonlinear Phenomena* **4**, 139 (1982).

[24] J. Gibbon, M. McGuinness, «The real and complex Lorenz equations in rotating fluids and lasers», *Physica D: Nonlinear Phenomena* **5**, 108 (1982).

[25] A. Fowler, J. Gibbon, M. McGuinness, «The real and complex Lorenz equations and their relevance to physical systems», *Physica D: Nonlinear Phenomena* **7**, 126 (1983).

[26] H. Zeghlache, P. Mandel, «Influence of detuning on the properties of laser equations», *J. Opt. Soc. Am. B: Opt. Phys.* **2**, 18 (1985).

[27] J. Liu, S. Liu, «Complex modified function projective synchronization of complex chaotic systems with known and unknown complex parameters», *Appl. Math. Modell.* **48**, 440 (2017).

[28] O. E. Rössler, «An equation for continuous chaos», *Phys. Lett. A* **57**, 397 (1976).